2.2

SENSITIVITY OF OROGRAPHIC PRECIPITATION TO CHANGING SOIL MOISTURE AND AMBIENT CONDITIONS

S. Anquetin*, Eddy Yates, Vincent Mano
Laboratoire d'étude des Transferts en Hydrologie et Environnement (LTHE)
Grenoble, France

1. INTRODUCTION

Understanding the physical processes that lead to orographic precipitation has its importance in domains such as weather and climate prediction or water management. Mountains affect atmospheric circulation over a wide range of scales, contributing to an uneven repartition of moisture and rain in space and time. Understanding the link between temporal and spatial variations of rainfall distribution over complex terrain is therefore a great challenge for hydrological purposes. The runoff production of mountainous watersheds will be, therefore, very sensitive to this distribution.

Based on the analysis of radar images and non-hydrostatic simulations of a shallow convection case above the Cévennes - Vivarais region in the Southeastern part of France, Miniscloux et al. (2001), Cosma et al. (2002) and Anquetin et al. (2003) have shown that the small orographic features of the topography focus and intensify the precipitation due to the convergence of low level air masses within the succession of oriented ridges and valleys.

Following these previous works, this study is based on ideal atmospheric simulations that aim of understanding and highlighting the main processes that lead to orographic precipitation organized in bands. The interaction between the atmospheric flow conditions (wind direction, vertical shear) and the resulting precipitation is investigated in terms of location and intensity of the rain patterns. The role of initial soil moisture is also investigated and its contribution to the enhancement of shallow convection is presented in this abstract.

2. NUMERICAL DESIGN

The simulations were carried out with the 3D non-hydrostatic model MesoNH, developed jointly by Météo-France (CNRM) and the Laboratoire d'Aérologie (Lafore et al., 1998). Each simulation was performed over nine hours, using the grid nesting technique in its two-way formulation (Stein et al., 2000). Figure 1 presents the topography for the two nested domains at 4km and 1km respectively. Table 1 gives a summary of the main numerical characteristics of the simulations.

*** *Corresponding address:*** Sandrine Anquetin, L.T.H.E, BP 53, 38041 Grenoble Cedex, France, email: sandrine.anquetin@hmg.inpg.fr

	Dad domain	Son domain
Horizontal resolution (km)	4	1
Vertical resolution (m)	Gal-chen and Sommerville (1975) 60m (ground) to 1000m (top)	
Size of the domain (points)	80x90x45	80x180x45
Time step (s)	12	3

Table 1 : Numerical configuration of the simulations

No subgrid-scale convection is used due to the high resolution of the grids; the convection is therefore explicitly solved. To simulate shallow convection under warm environment, the standard Kessler scheme (Kessler, 1969) is used to characterize the microphysical processes and the rain production. It governs the equation of three water species mixing ratios (vapour, cloud water, rain water). The mixing length and the turbulent kinetic energy are provided by the Bougeault and Lacarrère (1989) scheme. The ground fluxes are given by the ISBA model (Noilhan and Planton, 1989). The heat and water transfers are explicitly taken into account within the ground, described with three layers. If no particular mention, the initial relative humidity of the soil is fixed to 50%.

For all the simulations, the initial state of the atmosphere is prescribed by the same idealized sounding. The first 4km-depth layers are conditionally unstable ($N=0.008s^{-1}$, RH=80%), then we impose a stable stratified layer between 4 and 10km ($N=0.02s^{-1}$, RH varies linearly between 80 at 4km to 50% at 10km). The top of the domain (up to 20km) remains stable ($N=0.01s^{-1}$) and becomes dryer (RH=0% at 20km).

The simulations differ with the prescribed upstream flux (zonal and meridian winds, vertical shear) and the soil moisture content. Table 2 presents the six numerical experiments performed to evaluate the sensitivity of the orographic precipitation to atmospheric and ground forcings. The last column highlights how the water content in the soil varies during the simulation: i) freely and governed by the transfers modelled by ISBA; ii) maintained fixed to a given state (Dry or Saturated).

Exp. Name	Zonal Wind (m/s)	Meridian Wind (m/s)	Altitude (km)	Soil state given by:
Reference				
Sref	0	15	0 – 20	ISBA
Impact of the ambient conditions				
SW10	2,6	14,8	0 - 20	ISBA
SE10	-2,6	14,8	0 - 20	ISBA
VShear	0 Linear evolution 0	15 30	0 – 1.5 1.5 - 5 > 5	ISBA
Impact of the ground forcing State of the ground in the mountainous area (above 300m)				
Mdry	0	15	0 – 20	Dry
Mwet	0	15	0 - 20	Saturated

Table 2 : Characteristics of the numerical experiments

The atmospheric flux and the state of the ground (if explicitly prescribed) remain constant during the nine simulated hours. The seven first hours are used for the spin-up of the two models. The two last hours are explicitly analysed using simulated fields recorded every 10mn. Here, we analyse only the fields simulated in the small domain during the two last hours.

The simulated fields are analyzed through the geostatistical analysis developed by Miniscloux et al. (2001). The main results are discussed below.

3. ROLE OF THE ATMOSPHERIC FORCING

3.1 Mean rain fields associated to shallow convection

The mean rain intensity maps are presented in Figure 2. The SW10, SE10 and VShear simulated precipitation fields are compared to the reference simulated rainfall (Sref). The global structure of the four simulated rain fields is organized in bands oriented in the main atmospheric flux direction. The vertical extension of the clouds (not presented here) does not exceed 4 to 4.5km for the four simulations. Under these atmospheric forcings, convection is then triggered by the topography. Its horizontal and vertical structures reveal that we are faced to orographic shallow convection as observed by Miniscloux et al. (2001) and Kirshbaum and Durran (2005), and simulated by Cosma et al. (2002), Anquetin et al. (2003) and Kirshbaum and Durran (2004).

3.2 Impact of the upstream wind direction

To investigate further the impact of the atmospheric upstream conditions on the resulting rain field (location, intensity, shape), a Lagrangian approach (Miniscloux et al., 2001) is used to analyse the simulated fields. The purpose is to compute the mean underlying topography around the triggering point of the rain cells and the corresponding mean rain field. A rain cell is defined as a connected set of contiguous points for which the rain exceeds the given threshold of 10mm.h^{-1}. In Figure 3, the mean statistical simulated rain fields and the corresponding mean underlying topography are presented for the four experiments. The highest rain intensities are concentrated to the southern edge of orographic cells. The rain patterns are deflected toward east according to the general orientation of the topography (Miniscloux et al., 2001; Cosma et al., 2002). The shape of the statistical rain field under the SW10 atmospheric condition is longer and larger compared to the Sref precipitation pattern whereas the resulting SE10 rain field has a wider shape and is less intense.

The impact of the direction of the upstream flux is not perceptible on the mean cumulated rainfall over the whole domain, which remains almost the same for the Sref, SW10 and SE10 experiments.
Nevertheless, the rainfall maximum is more sensitive to the upstream wind conditions. The wind direction oriented South-West (SW10, only ten degrees to the west compared to the reference Sref) leads to a 40% increase of the maximum of precipitation. The SE10 experiment (ten degrees eastward compared to the reference Sref) reveals a decreas of almost 11% of the maximum of precipitation compared to the reference. These differences are only due to the differences between the topographies “seen” by the upstream fluxes. Indeed, the capability of the air masses to form precipitation will be essentially governed by the way the upstream flow will reach a given topography (link between the orientation of the flux and the main slope direction of the topography). In this case, under the SE10 atmospheric conditions, the mean slopes “seen” by the flux are the highest because we are closer to the normal of the mean mountain crest. Nevertheless, the triggering rain is the lowest. Using the Lagrangian analysis where the mean low-level divergence of the flux is calculated centred on the triggering point, we observed (not shown in this paper, Yates (2006)) that above the highest mean slope region, for the SE10 conditions, the atmospheric flux is divergent due to the topographic bypass. As shown by Anquetin et al. (2003), the low-level convergence is essential to enhance shallow convection in mountainous areas. Therefore, for this case, behind the obstacle, the convergence leads to the formation of precipitation shifted North-eastward (Figure 4). The resulting precipitation pattern becomes wider and less intense than for the Sref and SW10 experiments.

3.3 Impact of the vertical shear

Figure 3, the vertical shear (VShear experiment) leads to the formation of longer and narrower rain cells and more intense rainfall than for Sref and even SW10.
But, the simulated cumulated rainfall amount is 40% less than the reference’s one. This is essentially due to the area of no convection located on the abscissas

between 720 and 760km extended Lambert II coordinates (Figure 2).
To investigate further the impact of the wind shear on the formation of the convection, the Lagrangian analysis is used in order to evaluate the horizontal vorticity in the first grid cell calculated above the triggering points. To explain the inhibition of the convection between 720 and 760km (Figure 2), we perform the same Lagrangian analysis in this restricted area taking the triggering points of the Sref simulation.
In the convection area, the horizontal vorticity for the VShear flux above the triggering points is 50% larger than the one evaluated in the restricted area (not shown here). The flow is therefore more 3D. In the restricted area, the horizontal vorticity for the VShear flux above the Sref triggering points is less than the one calculated based on the Sref flux. The vertical shear remains approximately in a 2D plane.
These results strengthen some previous works (Asai, 1964; Kirshbaum and Durran, 2004).
Asai (1964) showed that the 2D vertical shear limits the production of the convection due to the conversion of the vertical kinetic energy into kinetic energy for the main flow. The convective movements are therefore no more in phase with the temperature perturbations leading to a smaller conversion of the available potential energy (CAPE) into kinetic energy. In the no-convection area, the VShear low-level flow is slightly deflected to the west compared to its previous direction, but the 2D shear remains important and contributes to the inhibition of the shallow-convection production (Figure 5-a).
When the vertical shear is associated to a rotation of the air masses, the convection is therefore enhanced (Kirshbaum and Durran, 2004) even on a real topography as show in this work (Figure 5-c).

4. IMPACT OF THE SOIL MOISTURE

In this part, the role of the soil moisture on the rainband intensity is discussed based on the results of Sref, Mdry and Mwet simulations. While the ground water content during the Sref simulation varies from its initial state prescribed at 50% of its field capacity, during the Mdry and Mwet simulations, the water content is maintained fixed whatever the precipitation rate is. For the Mdry simulation, all the ground above 300m altitude is maintained dry whereas the ground of the plain (below 300m altitude) is kept saturated. For the Mwet simulation, the ground conditions are the opposite.

4.1 Mean rainfall fields

As in the previous section, the mean simulated rain field is organized in bands taking place in the mountainous area (Yates, 2006). At regional scale, we do not observe any revealing signature of the soil moisture on the mean rainfall. The rain band structure is located approximately at the same place for the three simulations. The mean cumulated rain fields are almost the same. The maximum of precipitation is larger for the Mdry simulation (21% larger than the reference's one). The rain cell advection and the cell triggering within the bands are approximately the same for the three simulations. We observe a small impact of the saturated state of the ground in the mountain (Mwet) leading to an attenuation of the rain triggering. The shape of the bands is approximately identical for the three simulations. Nevertheless, the Mwet ground conditions lead to the formation of much smaller rain cells.

4.2 Local instability of the low-level atmospheric layers

Figure 6 presents the rainfall intensity within a common band for the three simulation in the mountainous area (AA' transect showed Figure 6-a). In Figure 6-b and 6-c, the Mdry and Mwet simulated rainfall intensities (solid lines) are compared to the Sref simulated rainfall intensities (dotted lines), respectively.
While at regional scale, no specific signature of the soil moisture appears, Figure 6 shows a strong impact of the ground forcing on the rainfall intensity along the transect.
Figure 6-c, the simulated peaks for the Mwet conditions are on the same order of the reference's one, but are slightly shifted to the south. Due to the type of the soil in this region, shallow and permeable, the Sref state of the ground reaches saturation after 9 hours. Therefore, the ground conditions for Mwet and Sref become very close in the mountainous area.
Figure 6-b, the simulated peak under the Mdry conditions is more than 3 times larger than the reference's one, and is slightly shifted to the north.
To identify the origin of this enhancement, the vertical structure of the atmosphere is studied based on three soundings at RS1, RS2 and RS3 locations, presented in Figure 6. In the hilly sector (between 300 and 500m altitude, sounding RS1), the soundings for Sref, Wdry and Mwet simulation conditions are identical (Yates, 2006). The shallow convection is only due to the orographic uprising and the presence of the small scale topographic features. Below 300m altitude, the ground state is maintained to saturation in the Mdry simulation. This state does not have any impact on the low-level stratification which remains approximately the same than the one prescribed at the upstream boundary.
In Figure 7, the soundings at RS3 (mountainous area) are drawn for the Mdry and Mwet simulations (solid line) and compared to the reference (dotted line).
In the mountainous area, the soil moisture signature is more important leading to differences within the vertical structure of the atmosphere close to the ground.
In Figure 7-a, the dry state of the ground increases the instability of the low-level layers that are more saturated (due to the upstream condition where the ground of the plain is maintained saturated). This effect is readable up to 820hPa, and it explains the higher peak value in this region (Figure 6-b).

In Figure 7-b (Mwet simulation), the first atmospheric layers above the ground (up to 850hPa) are again more unstable and more saturated than the reference. Nevertheless, a stronger inversion (around 820hPa) reduces the vertical extension of the convection and leads to dryer air masses above. The resulting rain peak remains approximately the same than the reference's one.

A complementary study (Yates, 2006) based on the Lagrangian analysis of the vertical gradients of the potential temperature and of the adiabatic wet-bulb potential temperature strengthens these results and makes them more general. The soil moisture does not control the triggering processes but modifies their amplitude.

5. CONCLUSIONS

A number of idealized simulations of the atmosphere surrounding the Cévennes – Vivarais topography (southeast of France) were done, with changing upstream flow direction, shear and soil moisture content. The main objective was to highlight the interaction between the local atmospheric flow and the surface forcing on the resulting precipitation associated to shallow convection. This type of convection is organized in rain bands triggered by the orographic uprising and maintained by the small scale features of the relief.

The location, the triggering and the intensity of the convective rain cells strongly depend on the upstream wind direction. The shallow convection processes will be more or less active according to the topography "seen" by the air masses.

Three-dimensional shear enhances shallow convection whereas vertical shear remaining almost in the same plan limits the convective processes.

Soil moisture content has little impact on the regional mean resulting precipitation and on the location of the bands. Within the rain bands, ground forcing can modify the atmospheric stratification up to 1.5km above the ground leading to a local enhancement of the precipitation.

These idealized simulations might be completed with simulations forced with real atmospheric conditions in order to evaluate the cumulated rain associated to shallow convection in the Cévennes – Vivarais region. To complete previous studies (Cosma et al., 2002; Anquetin et al., 2003) based on the simulation of one real case of shallow-convection, the objective is to evaluate the contribution of the orographic rain in the general pluviometric regime of this region. This might be done based on a weather regime approach.

Acknowledgements. The current study has been supported by the PATOM and the ECCO-PNRH research programs of the CNRS-INSU, the French Institute for the Universe Sciences. The numerical simulations were carried out on the NEC of the IDRIS (CNRS) computing centre.

6. REFERENCES

Anquetin, S., F. Miniscloux, J.-D. Creutin, and S. Cosma, 2003, Numerical simulation of orographic rainbands, J. of Geophysical Research, 108(D8), 8386, doi:10.1029/2002JD001593.

Asai, T., 1964, Cumulus convection in the atmosphere with vertical wind shear: numerical experiment. J. Meteoro. Soc. Japan, 42, 245 – 258.

Bougeault, P. and P. Lacarrère, Parameterization of orographic induced turbulence in a mesobeta scale model. Mon. Wea. Rev., 117, 1872-1890, 1989.

Cosma, S., E. Richard and F. Miniscloux, 2002, The role of small-scale orographic features in the spatial distribution of precipitation, Q. J. Roy. Meteor. Soc., 128(579), 75-92.

Gal-Chen, T. & R.C.J. Sommerville, 1975 : On the use of a coordinate transformation for the solution of the Navier-Stokes equations, J. Comput.Phys., 17, 209-228.

Kirshbaum, D.J. and D.R. Durran, 2004, Factors governing cellular convection in orographic precipitation, J. Atmos. Sci., 61(6), 682-698.

Kirshbaum, D.J. and D.R. Durran, 2005, Observation and modelling of banded orographic precipitation, J. Atmos. Sci., 62(5), 1463-1479.

Lafore, J.P., J. Stein, N. Asencio, P. Bougeault, V. Ducrocq, J. Duron, C. Fischer, P. Héreil, P. Mascart, V. Masson, J.P. Pinty, J.L. Redelsberger, E. Richard and V.G. de Arellano, 1998 : The Meso-NH atmospheric simulation system. Part 1: adiabatic formulation and control simulations. Ann. Geophys., 16, 90-109.

Miniscloux, F., J.D. Creutin and S. Anquetin, 2001, Geostatistical analysis of orographic rainbands. J. of Applied Meteor., 40, 11, 1835-1854

Noilhan, J. and S. Planton, A simple parameterization of land surface processes for meteorological models. Mon. Wea. Rev., 117, 536-549, 1989

Stein, J., E. Richard, J.P. Lafore, J.P. Pinty, N. Asencio & S. Cosma, 2000 : High-resolution non-hydrostatic simulations of flash-flood episodes with grid-nesting and ice-phase parameterization. Meteor. Atmos. Physics, 72, 203-221.

Yates, E., 2006, Convection en région Cévennes-Vivarais : Etude de données pluviométriques, simulations numériques et validation multi-échelles, PhD thesis (in French), Institut National Polytechnique de Grenoble.

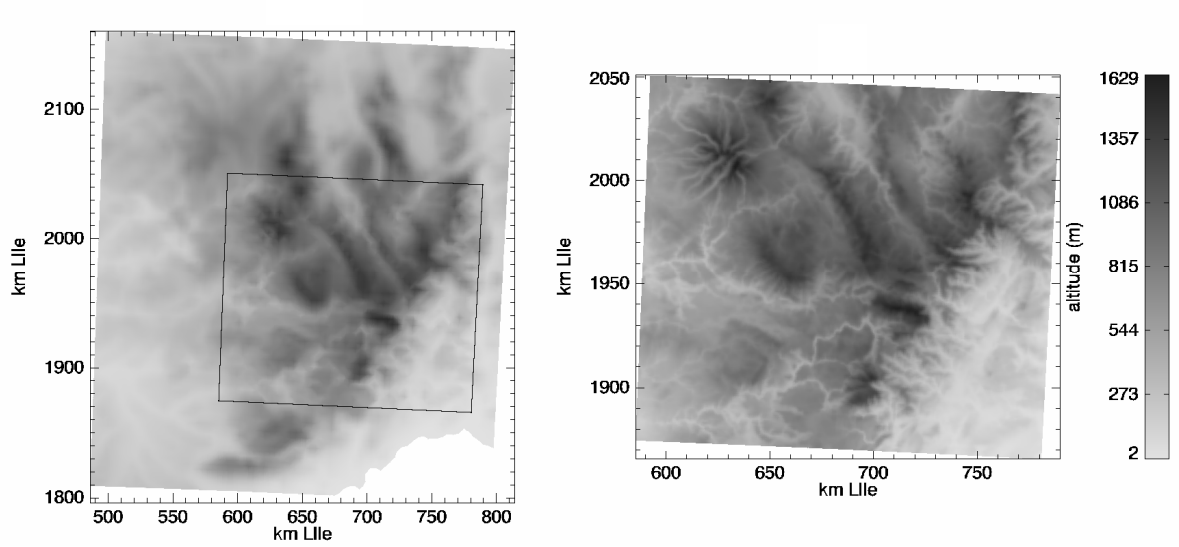

Figure 1: Topography of the two simulated domains, 4km and 1km grid resolution respectively. The black rectangle indicates the position of the nested domain within the larger domain.

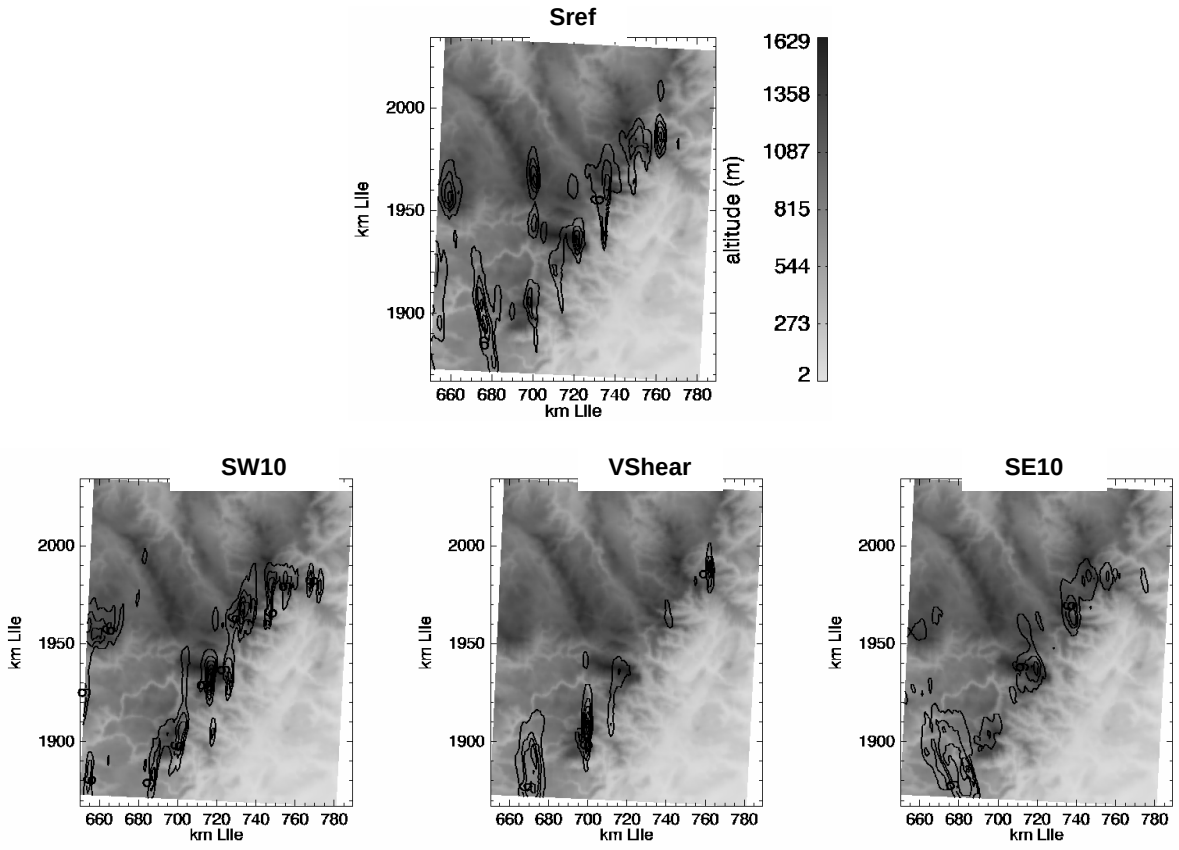

Figure 2: Mean simulated rainfall rates (solid line every 3mm.h^{-1}) for the Sref, SW10, VShear and SE10 experiments. The topography is represented in grey scale.

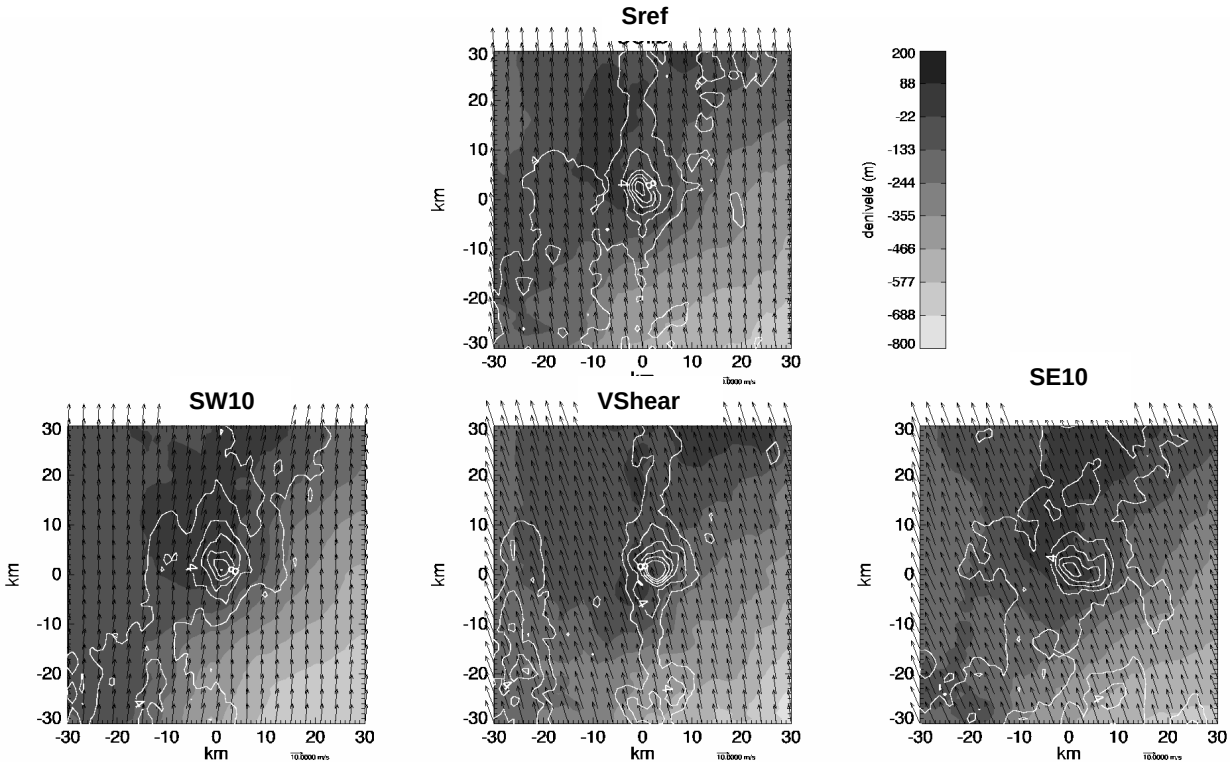

Figure 3: Mean statistical simulated rain fields (white solid lines, spaced by 2mm.h^{-1}) and the corresponding mean underlying topography (grey scale) centred on the triggering point (at (0,0)) of identified rain cells.

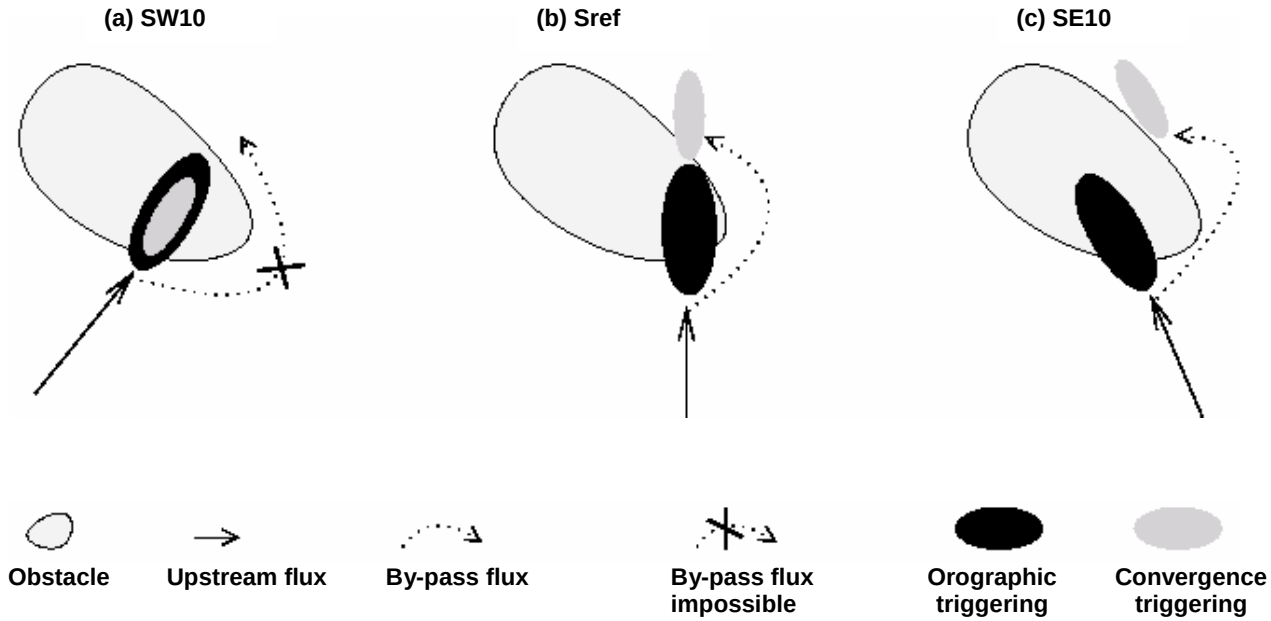

Figure 4: Impact of the wind direction on the precipitation triggering

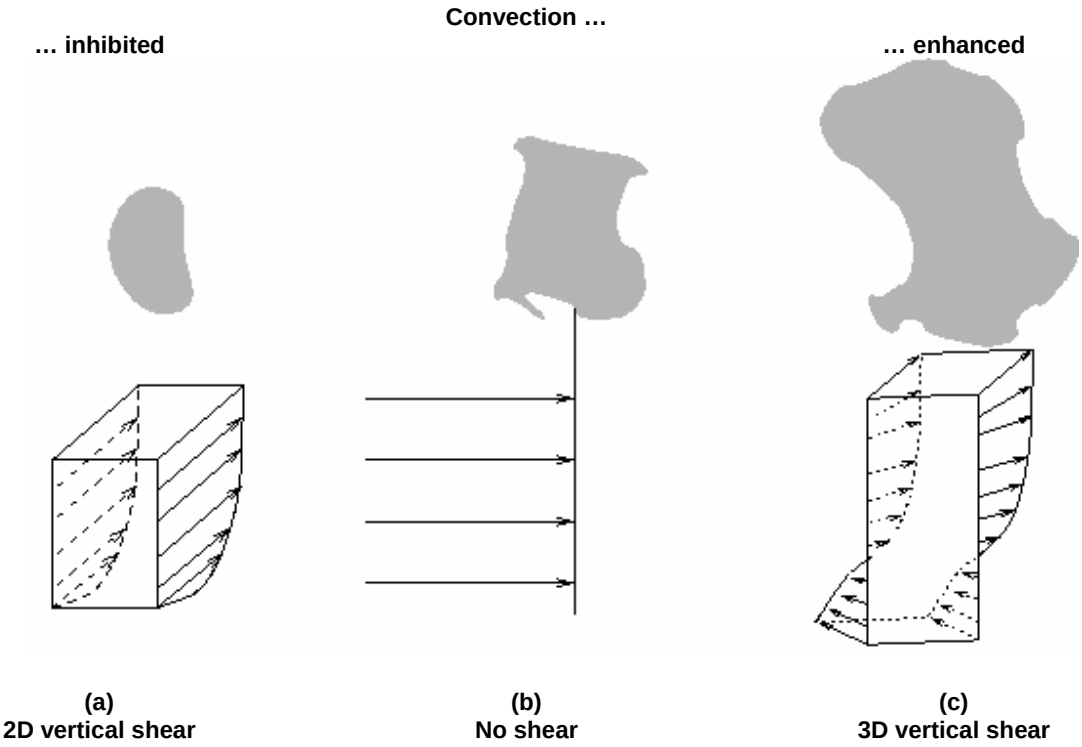

Figure 5: Impact of vertical shear on shallow convection production

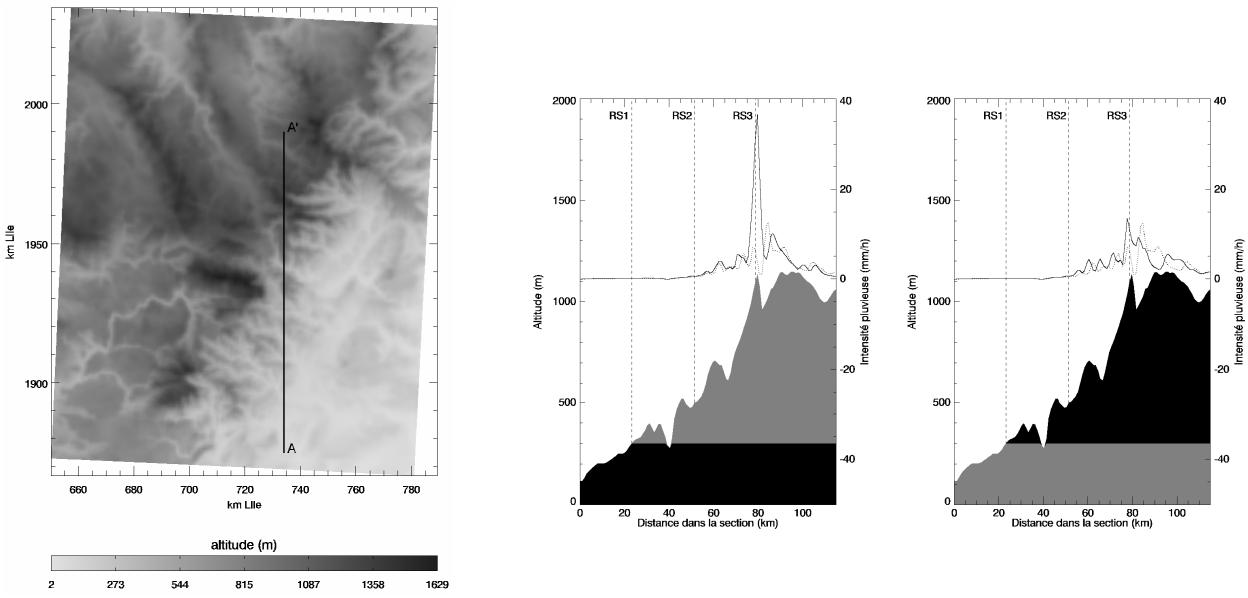

(a) **(b) Mdry** **(c) Mwet**

Figure 6: (b) and (c) Simulated rainfall rates for the Mdry and the Mwet simulations (solid line) compared to the simulated rainfall rate for the Sref simulation (dotted line) along the transect presented in (a). The black color indicates the part of the topography where the ground is saturated.

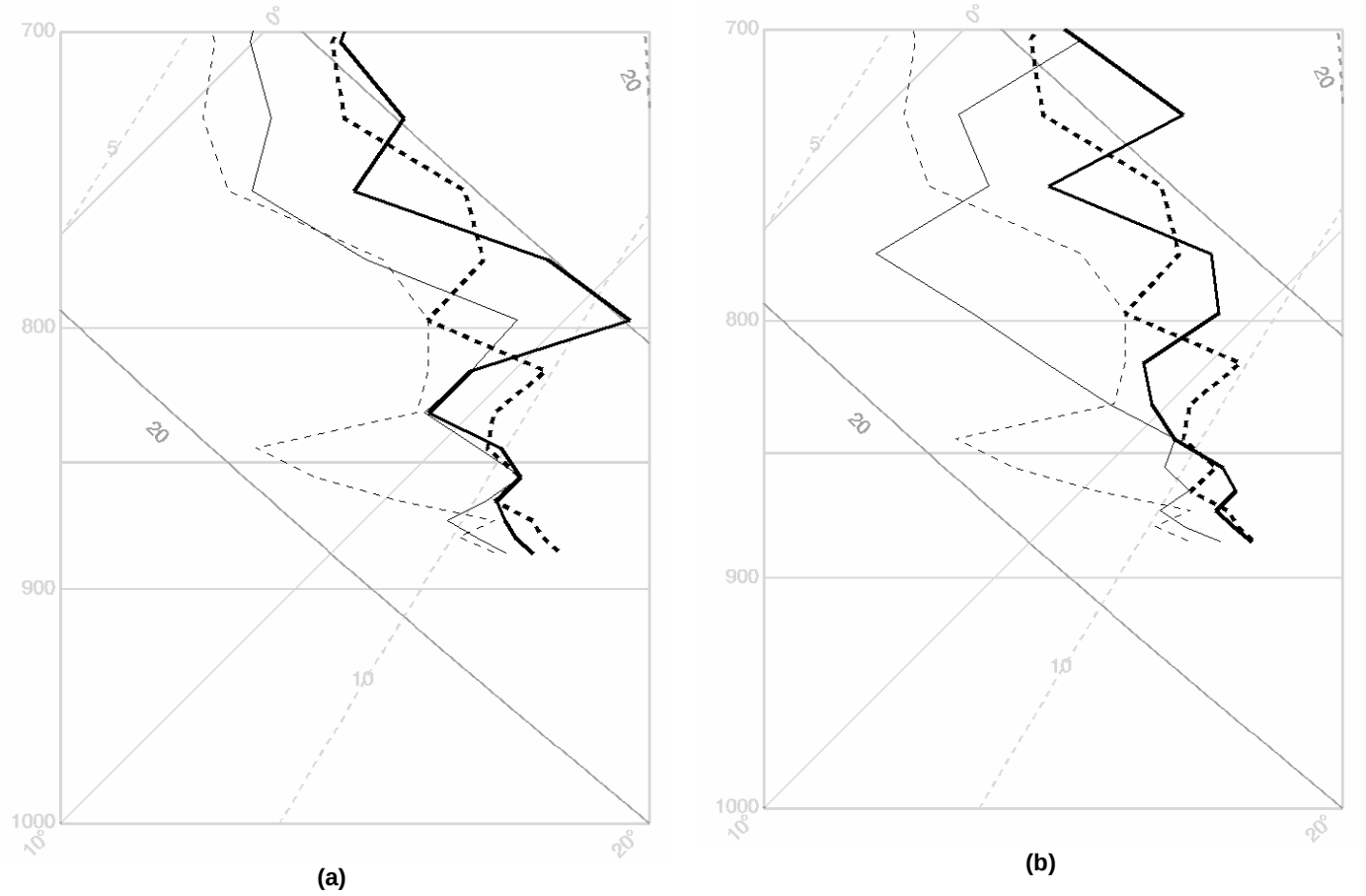

Figure 7: Comparison between the soundings at the RS3 location (Figure 6) for: (a) Mdry (solid line) and Sref (dotted line) experiments; (b) Mwet (solid line) and Sref (dotted line) experiments. The bold lines (solid and dotted) stand for the environmental curve whereas the thin lines are associated to the dew-point evolution.